Table S1. CRISPR and oligo sequences used for HRMA, sequencing, and whole mount *in-situ* hybridization (WISH) probe

Oligo Name	Sequence 5'-3'
sec23a gRNA	GGCCCGTCTTGCTGTGTACAAGG
sec23a^{uq23bh} HRMA FP	GCGAAAGCTTGTGTTCGAAGG
sec23a^{uq23bh} HRMA RP	CGGATGAGCTGTCTGTCCAA
sec23a^{uq23bh} sequencing FP	AATGGGGTGGTCAAAATAGGG
sec23a^{uq23bh} sequencing RP	CGAAAGCTTGTGTTCGAAGGT
col2a1a gRNA	GGAGGGGCCAGGAGGACCAC
col2a1a^{uq36bh} HRMA FP	TGGGTCAAAGATGCCATGTTGC
col2a1a^{uq36bh} HRMA RP	ATGCATTTACTTACAGGTGCTCCA
col2a1a^{uq36bh} sequencing FP	GAGGAATGTTTTGGAATGACGTGG
col2a1a^{uq36bh} sequencing RP	AGTGTGGGATTTGGGAGTTGG
mbtps1 gRNA	ACATTGCCAGGTTTTCATCC
mbtps1^{uq27bh} sequencing FP	CCTGTCACGCCCATACCATTA
mbtps1^{uq27bh} sequencing RP	CTAGCATTCTGCTCGCATCAC
mbtps1^{uq28bh} HRMA FP	GGTGTTGGAGGGATTGATTTTGAG
mbtps1^{uq28bh} HRMA RP	AAGGTGTCTGTCTGCCCTTTTTA
sec23a WISH FP	GCGCACCCATTCTGACAG
sec23a WISH RP	GGAATTAACCCTCACTAAAGGGAGAATCTCCGACCACCATGCCAG
sec23b WISH FP	CACACTTGTGAGCTTCAGGAAC
sec23b WISH RP	GGATCCATTAACCCTCACTAAAGGGAACGAACACGTAGCTCTTGGCGA

col2a1a WISH FP	TGCTGTGTGACGAGGTCAT
col2a1a WISH RP	GGAATTAACCCTCACTAAAGGGTTGCCTTGGAAACCTTGTG
cxcl12a WISH FP	AAAAAGCCCAACAGCAGCAGG
cxcl12a WISH RP	GGAATTAACCCTCACTAAAGACACGGAGCAAACAGGACTCC
cxcl12b WISH FP	ATCCTTGCTTTGTGGTCCAG
cxcl12b WISH RP	GGAATTAACCCTCACTAAAGTAGCGTTGTGTGACCAGAGG

Supplementary Figure 1

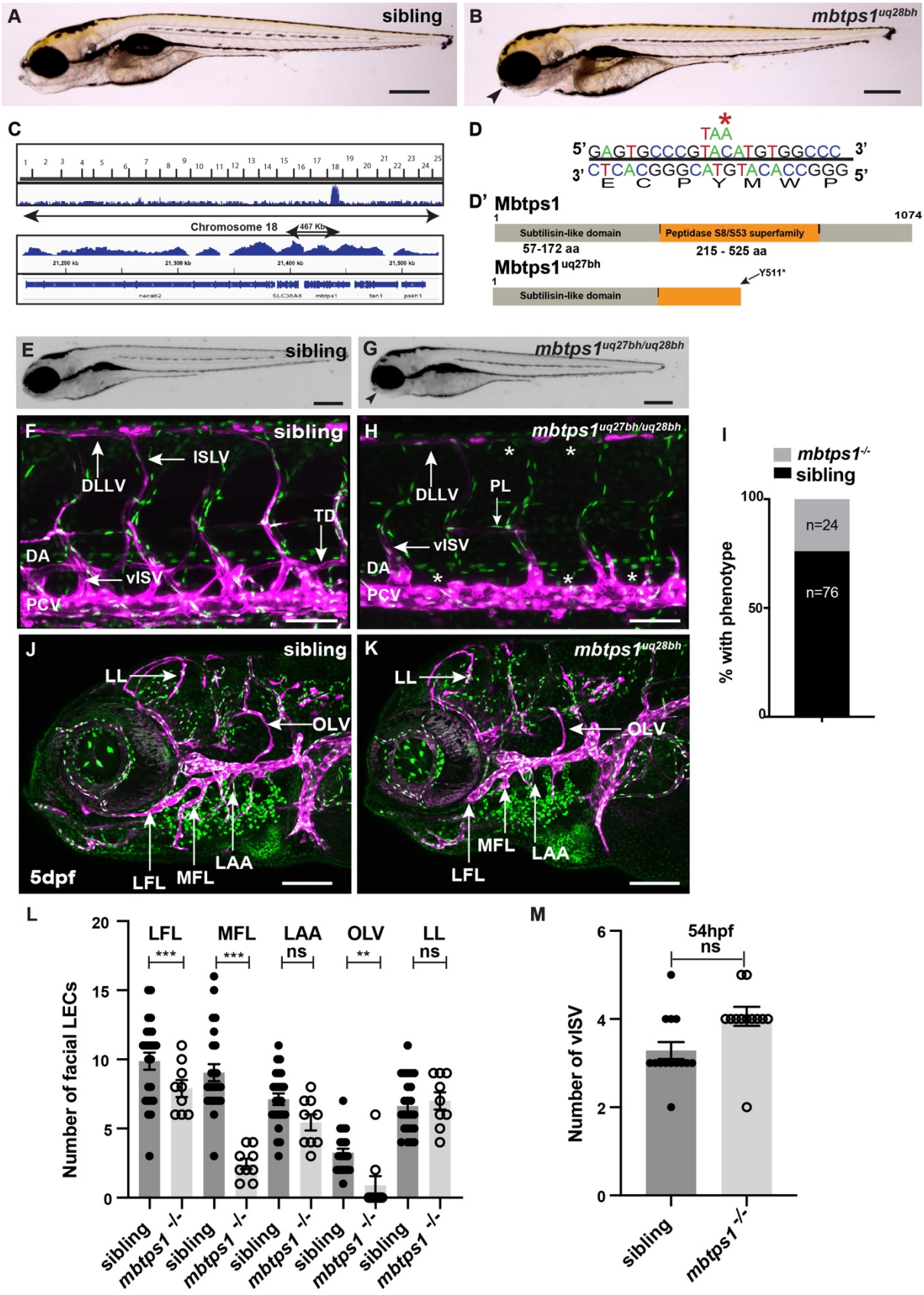

Fig. S1. Phenotyping and positional cloning of *mbtps1*^{uq27bh} using whole-genome sequence-based homozygosity mapping and mutation detection.

(A,B) Brightfield images showing shortened body axis and craniofacial defects in *mbtps1*^{uq28bh} mutant when compared to sibling at 5dpf. Black arrow indicates abnormal jaw structure. Bars, 50μm.

(C-D') Schematic plot of homozygosity across 25 chromosomes, shows a region of homozygosity on chromosome 18 containing *mbtps1* (A) with a C>A mutation introducing a premature stop codon at amino acid 511 in *mbtps1*^{uq27bh} (B, B').

(E-H) Brightfield and confocal images *Tg(fli1a:nEGFP); Tg(-5.2lyve1b:DsRed)* of sibling (E,F) and a *mbtps1*$^{uq27bh/uq28bh}$ compound heterozygous mutant (G,H). Short body axis, craniofacial defects (G) and loss of the lymphatic network (H) in compound mutants confirms *mbtps1* as the causative gene for the lymphatic defects observed at 5dpf. Bars, 50μm

(I) 24% of embryos from a complementation test showed mutant phenotype and were confirmed as compound heterozygous *mbtps1*$^{uq27bh/uq28bh}$ mutants (n=96 embryos scored).

(J-L) Confocal images *Tg(fli1a:nEGFP); Tg(-5.2lyve1b:DsRed) mbtps1*^{uq27bh} embryos. Siblings (J; n=20) display normal development of facial lymphatic vessels while *mbtps1*^{uq28bh} (K; n=6) have a significant reduction in the LFL, MFL, and at 5dpf (L). Bars, 30μm

LFL= lateral facial lymphatic; MFL= medial facial lymphatic.

(M) Quantification of vISVs at 54hpf reveals no difference between sibling (n=20) and *mbtps1*^{uq28bh} embryos (n=6). vISVs= venous intersegmental vessels.

*=P value<0.05, **=P value<0.01,***=P value<0.001.

Supplementary Figure 2

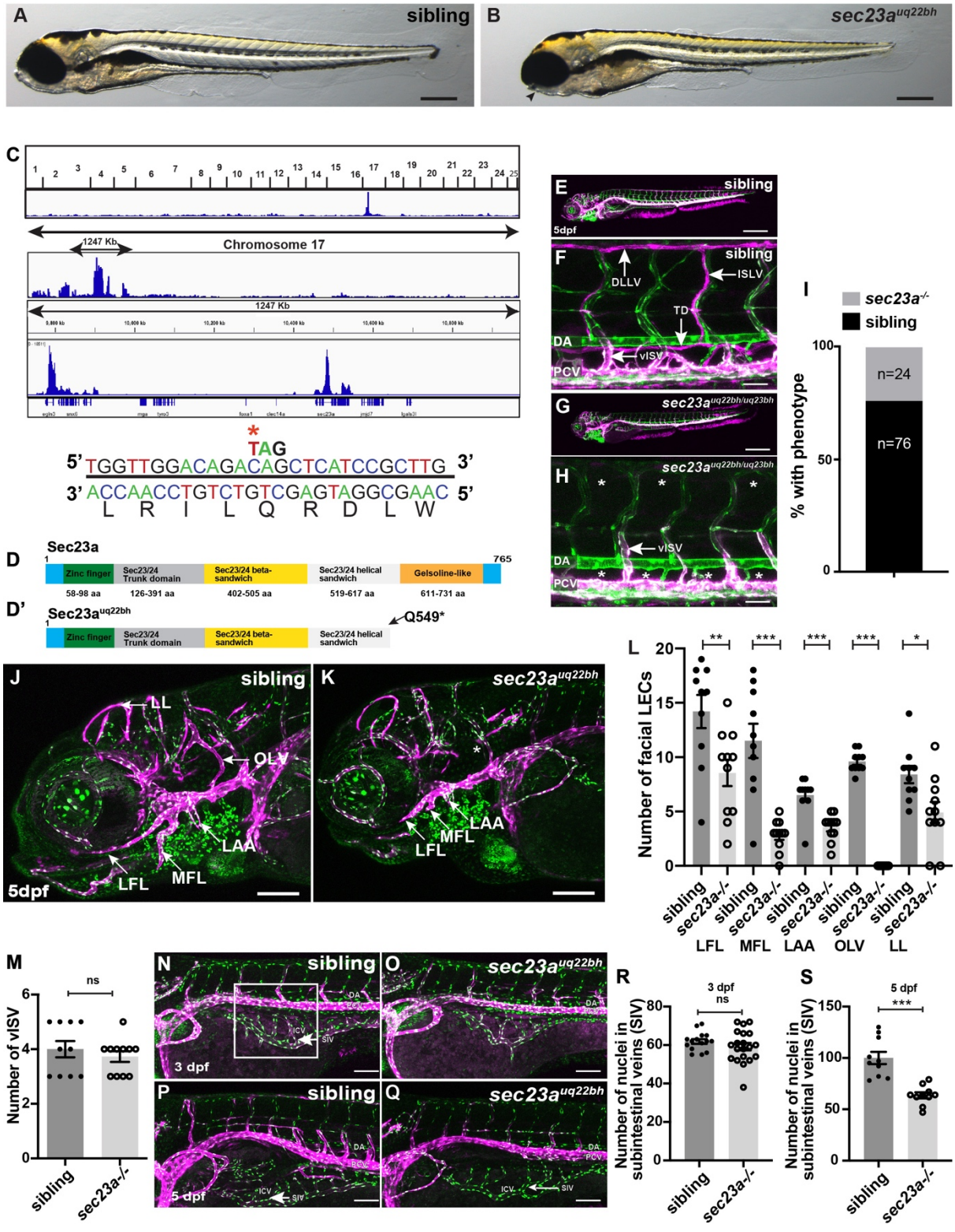

Fig. S2. Phenotyping and positional cloning of *sec23a*^{uq22bh} using whole-genome sequence-based homozygosity mapping and mutation detection.

(A,B) Brightfield images showing shortened body axis and craniofacial defects in a *sec23a*^{uq22bh} mutant when compared to sibling at 5dpf. Black arrow indicates abnormal jaw structure. Bars, 50μm.

(C-D') Schematic plot of homozygosity across 25 chromosomes, (C) shows linkage to chromosome 17 containing *sec23a*, with a C>T mutation (C) introducing a premature stop codon at amino acid 549 (D,D').

(E-H) Brightfield and confocal images of *Tg(kdrl:EGFP); Tg(-5.2lyve1b:DsRed)* sibling (E,F) and a *sec23a*$^{uq22bh/uq23bh}$ complementation test (G,H). The short body axis (G) and loss of the lymphatic network (H) in compound mutants confirms *sec23a* as the causative gene for the lymphatic defects observed at 5dpf. Bars, 50μm

(I) 24% of embryos from a complementation test showed mutant phenotype and were confirmed as compound heterozygous *sec23a*$^{uq22bh/uq23bh}$ mutants (n=96 embryos scored)

(J-L) Confocal images of *Tg(fli1a:nEGFP); Tg(-5.2lyve1b:DsRed)* *sec23a*^{uq23bh} embryos. Siblings display normal development of facial lymphatic vessels LFL, MFL, LAA, OLV, LL

LFL= lateral facial lymphatic; MFL= medial facial lymphatic; LAA = lateral branchial arches; OLV= otolithic lymphatic vessel; LL=lymphatic loop

(J,L) while *sec23a*^{uq22bh} have a significant reduction in LEC numbers in these vessels and a specific absence of the OLV at 5dpf (asterisk, K,L). Bars, 30μm

(M) Quantification of vISVs at 54hpf reveals no difference between sibling and *sec23a*^{uq23bh} embryos.

(N-Q) Confocal images of *Tg(fli1a:nEGFP); Tg(-5.2lyve1b:DsRed)* sibling (N,P; n=15) and *sec23a*^{uq22bh} (O,Q; n=20) intestinal gut vasculature at 3dpf and 5dpf showing *sec23a*^{uq22bh} mutants have relatively normal ongoing intestinal vascular development at 3dpf with mild delay at 5dpf. Bars, 30μm

(R,S) Quantification of the nuclei in the intestinal gut vasculature (within the white box) showed no difference in sibling (n=15) and *sec23a*^{uq22bh} (n=20) at 3dpf (R) however, at 5dpf (S) there was a mild reduction in *sec23a*^{uq22bh} (n=10) compared to sibling (n=10) suggesting late developmental delay after 3dpf.

*=P value<0.05, **=P value<0.01,***=P value<0.001.

Supplementary Figure 3

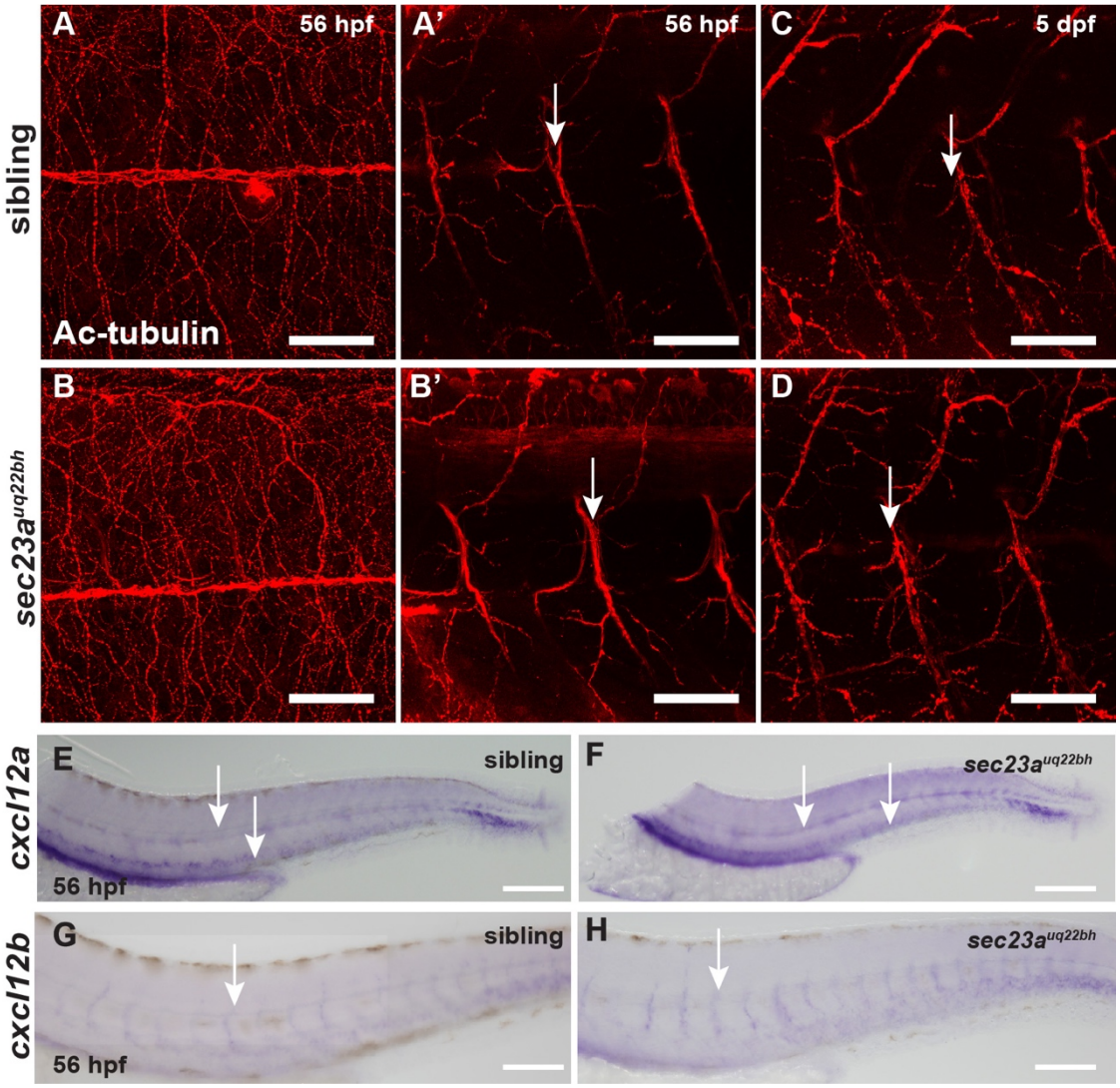

Fig. S3. *sec23a*^{uq22bh} mutants show no significant differences in motoneuron development and expression of chemokine ligands.

(A-D) Immunofluorescence assay showed normal expression of acetylated tubulin in motoneurons at 56hpf in siblings (A, A'; n=10), *sec23a*^{uq22bh} mutants (B, B'; n=10), 5dpf siblings (C; n=5) and *sec23a*^{uq22bh} mutants (D; n=5).

(E-F) Normal expression of *cxcl12a* was observed in the PCV in siblings (E; n=30) and *sec23a*^{uq22bh} mutants (F; n=10).

(G-H) *cxcl12b* expression was observed along arterial intersegmental vessels (aISVs) at 56hpf in siblings (G; n=30) and *sec23a*^{uq22bh} mutants (H; n=10).

Supplementary Figure 4

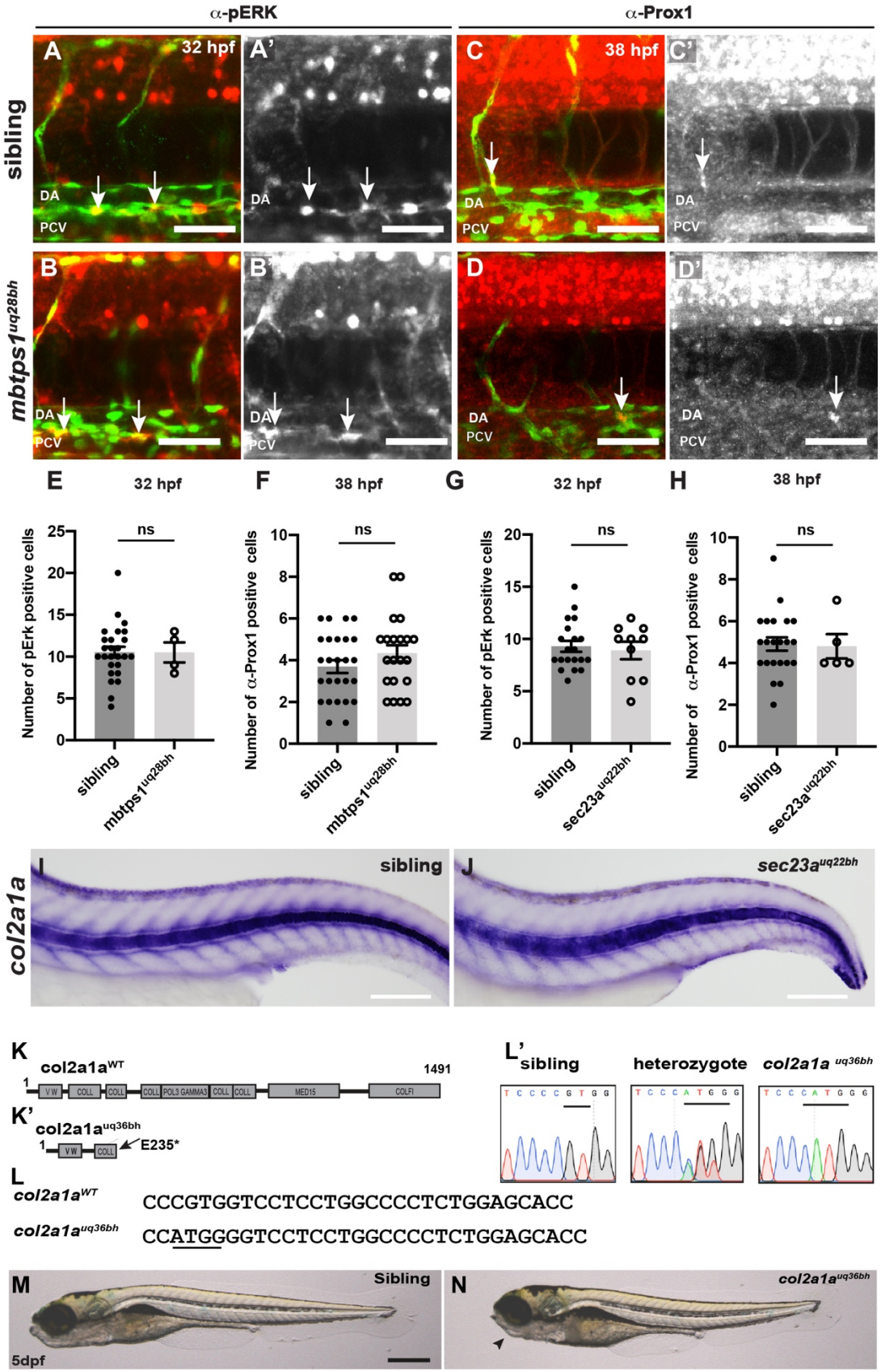

Fig. S4. *mbtps1*^{uq28bh} and *sec23a*^{uq22bh} mutants showed no significant differences in Prox1 and pErk expression in LECs

(A-B') Confocal images of *Tg(fli1a:nEGFP);* stained for eGFP (green) and p-Erk (red) in sibling (A; n=26) and *mbtps1*^{uq28bh} (B; n=4) (A', B' grayscale for pErk) at 32hpf showing the presence of pErk positive LECs (white arrows) on the dorsal side of the PCV.

(C-D') Confocal images of *Tg(fli1a:nEGFP);* stained for eGFP (green) and Prox1 (red) in sibling (C; n=26) and *mbtps1*^{uq28bh} (D; n=21) (C', D' grayscale for Prox1) at 38hpf showing the presence of Prox1 positive LECs (white arrows) on the dorsal side of the PCV.

(E,F) Quantification of pErk positive ECs (E) and Prox1-positive LECs (F) showed no significant difference between sibling and *mbtps1*^{uq28bh} embryos.

(G,H) No significant differences were observed on quantification of pErk positive LEC cells (G) and Prox1-positive LEC (H) between sibling and *sec23a*^{uq22bh} embryos.

(I,J) There was no difference in the expression of *col2a1a* in siblings (I; n=10) and *sec23a*^{uq22bh} mutants (J; n=10).

(K,L) CRISPR genome editing introduced a 3bp deletion/4bp (L,L') insertion and premature stop codon at amino acid 235 in *col2a1a*^{uq36bh} (K,K').

(M,N) Brightfield images showing short body axis in *col2a1a*^{uq36bh} when compared to siblings at 5dpf. Scalebars = 50μm

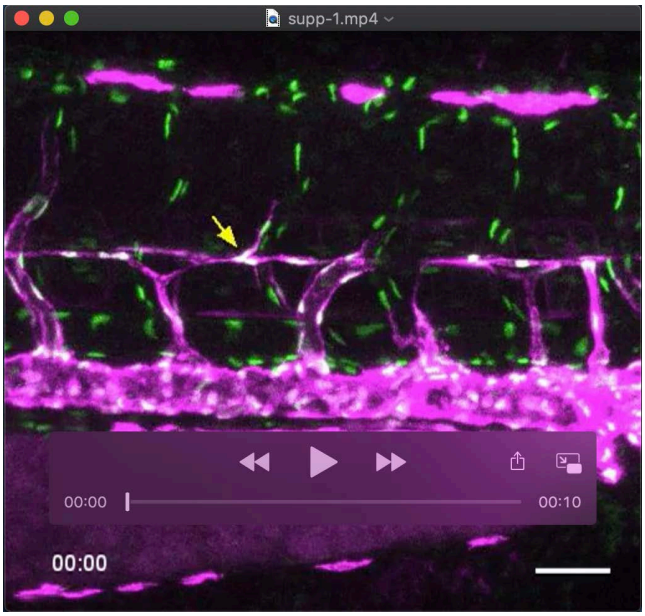

Movie 1. Time-lapse imaging of PLs in wildtype siblings from 65hpf to 78hpf. Arrow shows migration of PL dorsally

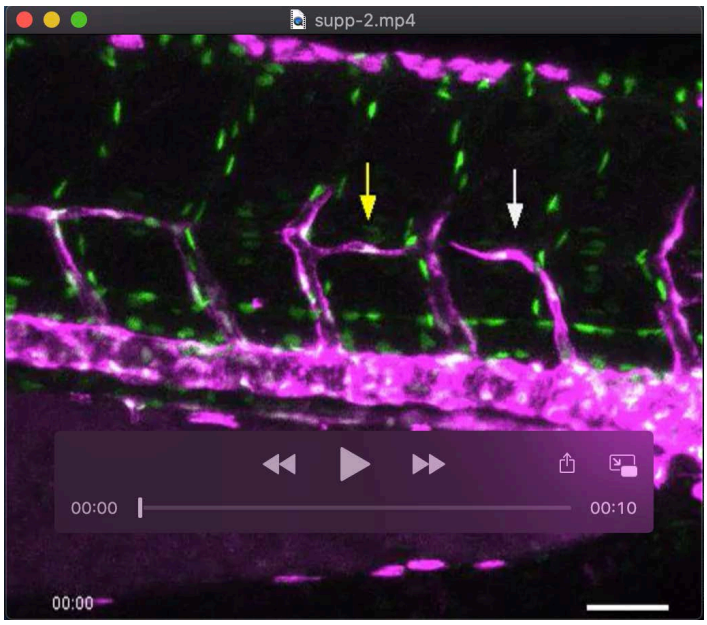

Movie 2. Time-lapse imaging of PLs in *sec23a*^{uq22bh} mutant from 65hpf to 78hpf. Yellow arrow shows a PL failing to migrate out of the HM. The white arrow shows a PL regressing.

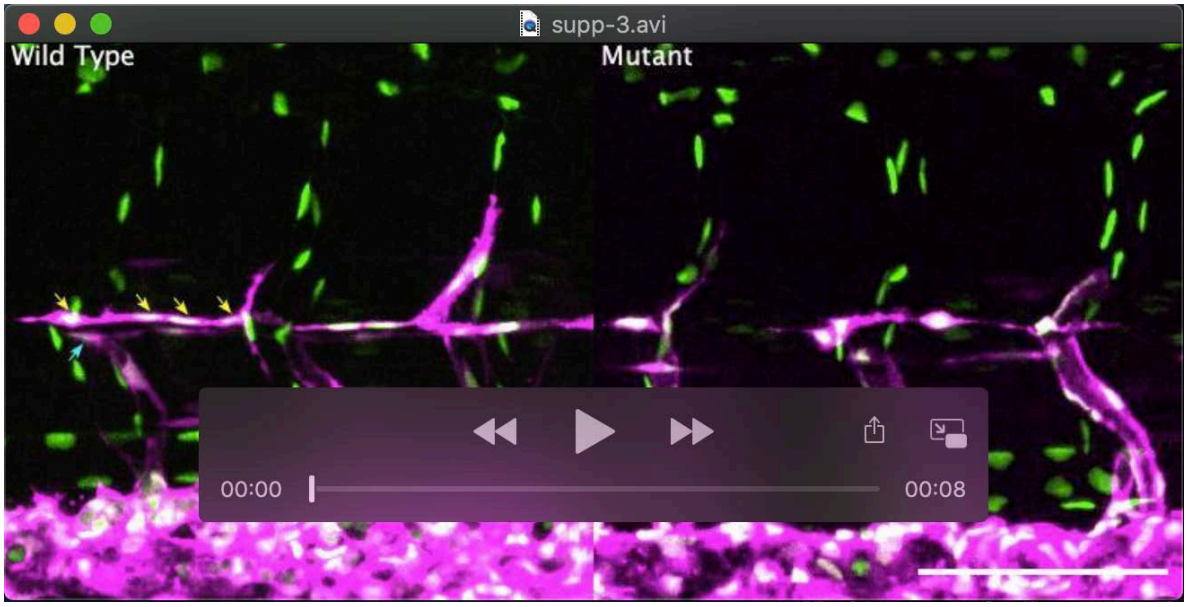

Movie 3. High speed spinning disk confocal time-lapse imaging of PLs in sibling (left panel) and *col2a1a*^{uq36bh} mutant (right panel) from 60-80hpf. Yellow arrows in the left panel highlight migration of LEC nuclei dorsally and blue arrows highlight migration ventrally. Representative of movies used to quantify phenotypes in Figures 4G & H.